Comparison of Fracture Healing Among Different Inbred Mouse Strains

Michaele B. Manigrasso · J. Patrick O'Connor

Abstract Quantitative trait locus analysis can be used to identify genes critically involved in biological processes. No such analysis has been applied to identifying genes that control bone fracture healing. To determine the feasibility of such an approach, healing of femur fractures was measured between C57BL/6, DBA/2, and C3H inbred strains of mice. Healing was assessed by radiography and histology and measured by histomorphometry and biomechanical testing. In all strains, radiographic bridging of the fracture was apparent after 3 weeks of healing. Histology showed that healing occurred through endochondral ossification in all strains. Histomorphometric measurements found more bone in the C57BL/6 fracture calluses 7 and 10 days after fracture. In contrast, more cartilage was present after 7 days in the C3H callus, which rapidly declined to levels less than those of C57BL/6 or DBA/2 mice by 14 days after fracture. An endochondral ossification index was calculated by multiplying the callus percent cartilage and bone areas as a measure of endochondral ossification. At 7 and 10 days after fracture, this value was higher in C57BL/6 mice. Using torsional mechanical testing, normalized structural and material properties of the C57BL/6 healing femurs were higher than values from the DBA/2 or C3H mice 4 weeks after fracture. The data indicate that fracture healing proceeds more rapidly in C57BL/6 mice and demonstrate that genetic variability significantly contributes to the process of bone regeneration. Large enough differences exist between C57BL/6 and DBA/2 or C3H mice to permit a quantitative trait locus analysis to identify genes controlling bone regeneration.

Bone fractures heal by a tissue regenerative process that involves a poorly understood pattern of temporal and spatial gene expression among several different cell types. Normally, fractures heal through an endochondral ossification process in which mesenchymal cells differentiate into chondrocytes and elaborate a calcified matrix that is replaced with bone to bridge the fracture [1]. Subsequently, the bone is remodeled via osteoclast and osteoblast activity to restore the material properties, morphology, and function of the broken bone. This process requires the concerted action of several cell types and biological processes, including chondrocytes, osteoblasts, osteoclasts, endothelial cells, inflammation, angiogenesis, chondrogenesis, osteogenesis, and bone remodeling. The genes that regulate or coordinate the complex interaction of these cell types to effect healing remain unknown.

Genetic analysis of fracture healing has relied upon testing candidate genes known to be involved in the various component processes of fracture healing. We found that fracture healing is significantly impaired in mice lacking cyclooxygenase-2 (*Ptgs2*, COX-2), a gene critical for normal inflammation or in rats treated with COX-2 inhibitors [2, 3]. Similarly, loss of proinflammatory tumor necrosis factor-α signaling also impairs fracture healing [4]. Other physiological processes also are necessary for bone regeneration. For instance, angiogenesis is critical for endochondral ossification and fracture healing is impaired in rats treated with angiogenesis inhibitors [5, 6].

M. B. Manigrasso · J. P. O'Connor (✉)
Department of Biochemistry and Molecular Biology,
UMDNJ-New Jersey Medical School and Graduate School
of Biomedical Sciences, 185 South Orange Avenue,
Newark, NJ 07103, USA
e-mail: oconnojp@umdnj.edu

A different approach to identifying genes that regulate fracture healing would be to identify quantitative traits of fracture healing that are extremely different between two inbred mouse strains. In turn, progeny from these two strains could be assayed for the quantitative trait in order to map the genetic loci responsible, ultimately leading to gene identification [7]. Typical quantifiable outcomes for fracture healing in animal models include histomorphometric measures of cartilage and new bone formation at the fracture site and physical testing of the healing bone to determine mechanical and material properties.

As a preliminary investigation into the feasibility of a quantitative trait locus approach to identifying novel genes involved in bone regeneration, we measured fracture healing in three different inbred strains of mice with well-characterized variations in bone mineral density and morphology (C57BL/6, DBA/2, and C3H) [8]. Fracture healing was measured using histomorphometry and torsional mechanical testing. The primary goal was to test the hypothesis that fracture healing varies between inbred mouse strains, indicating that bone regeneration is governed by genetic determinants. An additional goal was to identify a quantifiable trait that could be used to measure fracture healing differences between these strains and their progeny. The analysis indicates that significant differences in fracture healing occur between the three mouse strains tested and that the differences are sufficiently large to permit a quantitative trait mapping approach to identifying new genes involved in fracture healing.

Materials and Methods

Animals Used in This Study

Female C3H, DBA/2, and C57BL/6 (Taconic Farms, Germantown, NY) weighing 30.4 ± 3.0, 28.2 ± 2.9, and 30.1 ± 3.1 g, respectively, were used in this experiment. All animals were purchased as retired breeders and were approximately 6–9 months old at the beginning of the study. No significant differences in weight gain or loss following fracture were found between the mouse strains. Fracture healing occurs very rapidly in young rodents but slows with age [9–11]. Anticipating that it would be difficult to distinguish any healing differences in young mice, we chose to perform this initial analysis in older, retired breeder females. All experimental procedures were approved by the New Jersey Medical School Institutional Animal Care and Use Committee. Of the 248 mice used in this study, 127 were ultimately included in the radiographic, histological, histomorphometric, and mechanical analyses (Table 1).

Femur Fracture Model

Mice were anesthetized by an intraperitoneal injection of ketamine and xylazine (100 and 10 mg/kg, respectively). A closed diaphyseal fracture was produced in the right femur using a custom-made, three-point bending device (BBC Specialty Automotive Center, Linden, NJ) as described previously [12].

Radiography

Fracture healing was examined by dorsal–ventral radiographs of the mice. Radiographs were made of each mouse immediately postfracture to verify that a mid-diaphyseal fracture had been produced and once again at death to confirm that fracture reduction had been maintained. In addition, radiographs were made from a subset of mice at 7, 10, 14, 21, 28, and 42 days postfracture to establish a typical pattern of fracture healing for each strain. Radiographs were made using a model 804 Faxitron (Field Emission, McMinnville, OR) and Min-R 2000 mammography film (Eastman Kodak, Rochester, NY). Mice were either anesthetized or killed prior to radiography.

Histology and Histomorphometry

Animals used for histology were killed at 7, 10, 14, 21, 28, or 42 days postfracture. Following death, the fractured and contralateral control hindlimbs were dissected, cleaned of soft tissue without disturbing the callus, and fixed in 10% buffered formalin overnight. The femora were then embedded in polymethylmethacrylate, sectioned, and stained with van Gieson's picrofuchsin and Stevenel's blue, as described previously [12–14]. Samples were examined

Table 1 Disposition of the 248 inbred mice used in the study (data indicate number of mice)

Strain	Anesthesia deaths	Fracture destabilization	Poor fracture	Mechanical testing			Histology	
				Potting errors	User errors	Total analyzed	Poor quality	Total analyzed
C57BL/6	4	9	14	10	8	11	9	33
DBA/2	1	7	0	9	7	11	7	27
C3H	3	5	3	11	8	11	6	34

by light microscopy, and images were collected using an Olympus (Tokyo, Japan) BH-2 microscope and a Nikon (Tokyo, Japan) DXM1200f camera.

Histomorphometric measurements were made from microscopic images using ImageProPlus software (v. 5.0; Media Cybernetics, Silver Spring, MD). Measurements included total fracture area (TA), cartilage area (CA), fibrous granulation tissue area (GT, data not shown), mineralized tissue area (MA), and original femur bone area (B) in each fracture callus. Callus area (CALLUS) was calculated by subtracting the original femur bone from the total fracture area (TA − B = CALLUS). Because callus sizes varied depending upon the size of the femur for each mouse strain and the location of the sagittal section, MA and CA were normalized as the percentage of callus area (%MA and %CA). The endochondral ossification index was calculated by multiplying %MA by %CA. Theoretically, the endochondral ossification index could have a maximum value of 2,500 if %CA and %MA were 50% and a value of 0 if only cartilage or only mineralized tissue (bone) was present in the callus.

Mechanical Testing

The healing femurs and contralateral control femurs were tested to failure in torsion as described previously [12]. Briefly, mice were killed 28 days after fracture and the femurs dissected. Femur length, maximum diameter, and minimum diameter were measured. The distal and proximal ends of the femurs were cemented vertically in 0.25-inch hexagonal acorn nuts (Small Parts, Miami Lakes, FL) with cyanoacrylate glue (Electron Microscopy Sciences, Hatfield, PA). The acorn nuts were then filled with a self-curing acrylic resin (Seta-Tray; Accurate Set, Newark, NJ) to only expose the mid-diaphyseal region of the femur. Specimens were rehydrated after the potting process by allowing the potted femurs to soak in 0.9% saline for 1 hour prior to testing. Torsional testing was conducted using a servohydraulic testing machine (MTS, Minneapolis, MN) with a 20-Nm reaction torque load cell (Interface, Scottsdale, AZ). Femurs were tested by internal rotation to failure at an actuator head displacement rate of 1°/second and a data collection rate of 20 Hz. The peak torque and angle at failure were measured from the torque-angle deflection curves. From the callus dimensions, the polar moment of inertia (J) was calculated based upon a hollow ellipse model. Maximum shear stress and shear modulus were also calculated. The wall-thickness value used in all equations was taken by averaging wall-thickness measurements of 10 randomly chosen left (unfractured) femurs from each mouse strain that were embedded as described above and sectioned perpendicular to the long axis of the bone. Wall thickness was measured in four places for each specimen and then averaged. The average wall thickness for each specimen was then used to calculate an aggregate average wall thickness for each mouse strain. The aggregate averages and other femur dimensions are shown in Table 2. Only femurs harvested and tested without an adverse incident were used in the final calculations.

Statistics

Statistical analysis of the histomorphometric and mechanical testing data was performed using analysis of variance (ANOVA) with Holm-Sidak post-hoc tests, as required. Differences were considered to be significant at $P < 0.05$. Estimation of sample sizes was based upon t-test comparisons using the standard deviations (SDs) for all samples within a time point or outcome test. Statistical analyses were performed using SigmaStat 3.0 software (SPSS Inc., Chicago, IL). Effect sizes were calculated using Effect Size Generator software, version 4.1 (Clintools Software, Melbourne, Australia).

Results

Complications Associated with Fracture Production and Analysis

A large number of mice were excluded from this study for a variety of reasons (Table 1). Because all the fractured femur mechanical values were normalized to the contralateral,

Table 2 Physical dimensions of intact and healing femurs from different mouse strains (mean ± SD in millimeters)

Strain	Wall thickness	Length	Maximum diameter	Minimum diameter
C57BL/6				
Left (intact)	0.21 ± 0.03	15.49 ± 0.40	1.85 ± 0.13	0.93 ± 0.06
Right (fractured)	–	14.62 ± 0.74	3.64 ± 0.46	1.82 ± 0.23
DBA/2				
Left (intact)	0.28 ± 0.03	13.12 ± 0.29	1.73 ± 0.08	1.09 ± 0.07
Right (fractured)	–	12.76 ± 0.28	3.28 ± 0.37	2.50 ± 0.39
C3H				
Left (intact)	0.52 ± 0.05	14.97 ± 0.48	1.75 ± 0.10	1.47 ± 0.08
Right (fractured)	–	14.30 ± 0.63	3.47 ± 0.21	2.82 ± 0.27

intact femur, many samples were lost in which only one of the two mechanical tests failed. A common problem with the mechanical testing protocol occurred when polymethylmethacrylate cement trickled over the fracture site during the potting procedure (Table 1, "potting errors"). Another problem was simple handling of the fracture specimens, which were very delicate and easily broken ("user errors"). Mice from all strains were excluded because of fracture destabilization that occurred when the intramedullary pin was dislodged from the canal and no longer provided fracture stabilization. In addition, a large number of C57BL/6 mice were excluded because of poor fractures. The poor quality of bone in the C57BL/6 mice made it difficult to obtain diaphyseal fractures that were not initially comminuted. Many histological specimens were cut off-axis or overpolished during preparation and lost. Improvements in technique would reduce the number of lost specimens and increase the overall success rate. However, development of alternative assay methods that reduce specimen handling would likely increase the overall success rate and likely reduce assay variability.

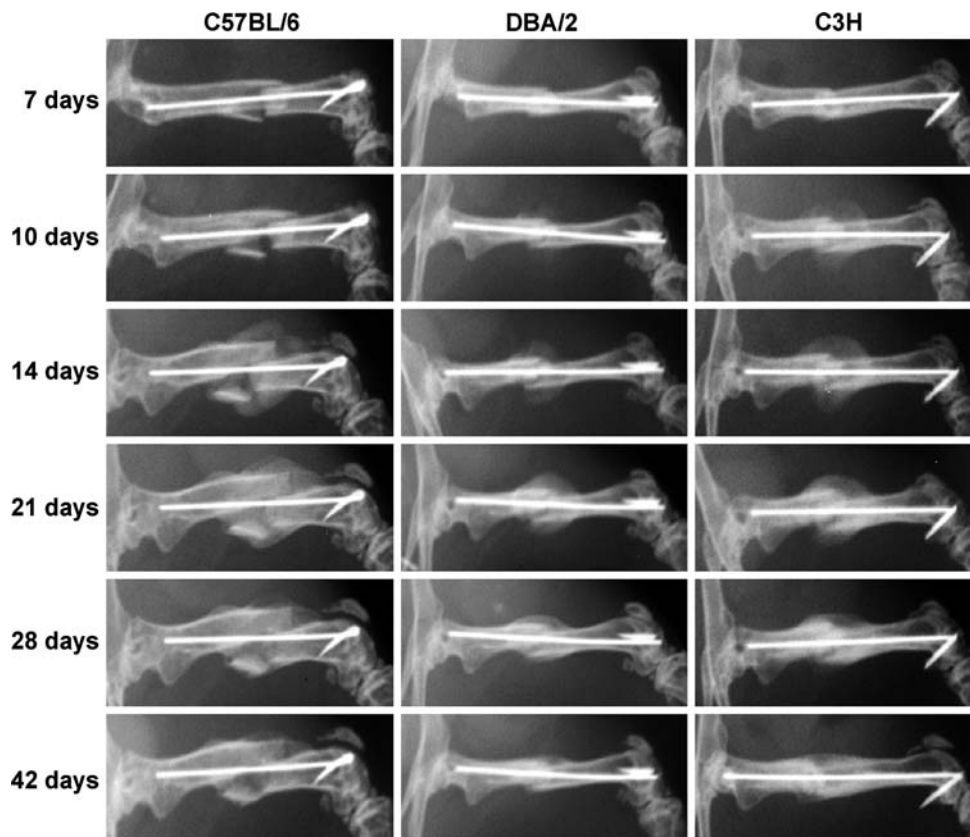Radiographic Comparison of Fracture Healing Between Inbred Mouse Strains

The pattern and timing of fracture healing were qualitatively followed for each strain using serial radiographs. As seen in Fig. 1, very little radiographic evidence of the fracture callus was evident 7 days after fracture. By 10 days, a mineralized callus was evident in the C3H and DBA/2 strains. The callus appeared to bridge the fracture site in all strains between 2 and 3 weeks after fracture, as has been previously reported for this fracture model [12]. Remodeling of the callus was apparent in the 4- and 6-week radiographs for all strains as callus size appeared diminished with a concomitant increase in radiographic density. A callus was still evident in all strains after 6 weeks of healing.

Histological and Histomorphometric Comparison of Fracture Healing Between Inbred Mouse Strains

Calcified histology was used to qualitatively compare fracture healing between the C57BL/6, DBA/2, and C3H strains. A typical endochondral ossification pathway of fracture healing was observed for each strain (Fig. 2). Fracture bridging appeared to occur by 3 weeks after fracture in all strains. One notable difference was the appearance of new bone at the callus periphery in the 7- and 10-day C57BL/6 fracture callus specimens compared to the others. Fracture healing was compared quantitatively between the inbred mouse strains by histomorphometric measurement of callus size, percent cartilage, and percent

Fig. 1 Radiographic comparison of fracture healing between inbred mouse strains. Serial radiographs were made of C57BL/6, DBA/2, and C3H mice at the indicated time points. An X-ray dense callus was apparent in each strain by 10 days after fracture. Fracture bridging appeared to occur in each strain by 21 days after fracture. Remodeling of the callus appeared to begin by 21 days after fracture based upon the reduction in callus size

Fig. 2 Histological comparison of fracture healing between inbred mouse strains. Fractured femurs from C57BL/6, DBA/2, and C3H mice were collected at the indicated times. Calcified sections were stained with Stevenel's blue (cartilage, deep blue) and van Gieson's picrofuchsin (bone and mineralized cartilage, red), and digital images of each specimen were captured. Fracture bridging was apparent in each strain by 21 days after fracture. Mineralized callus tissue was evident after 7 days of healing in C57BL/6 mice at the callus periphery. Bone regeneration appeared to occur through a normal endochondral ossification pathway in each mouse strain
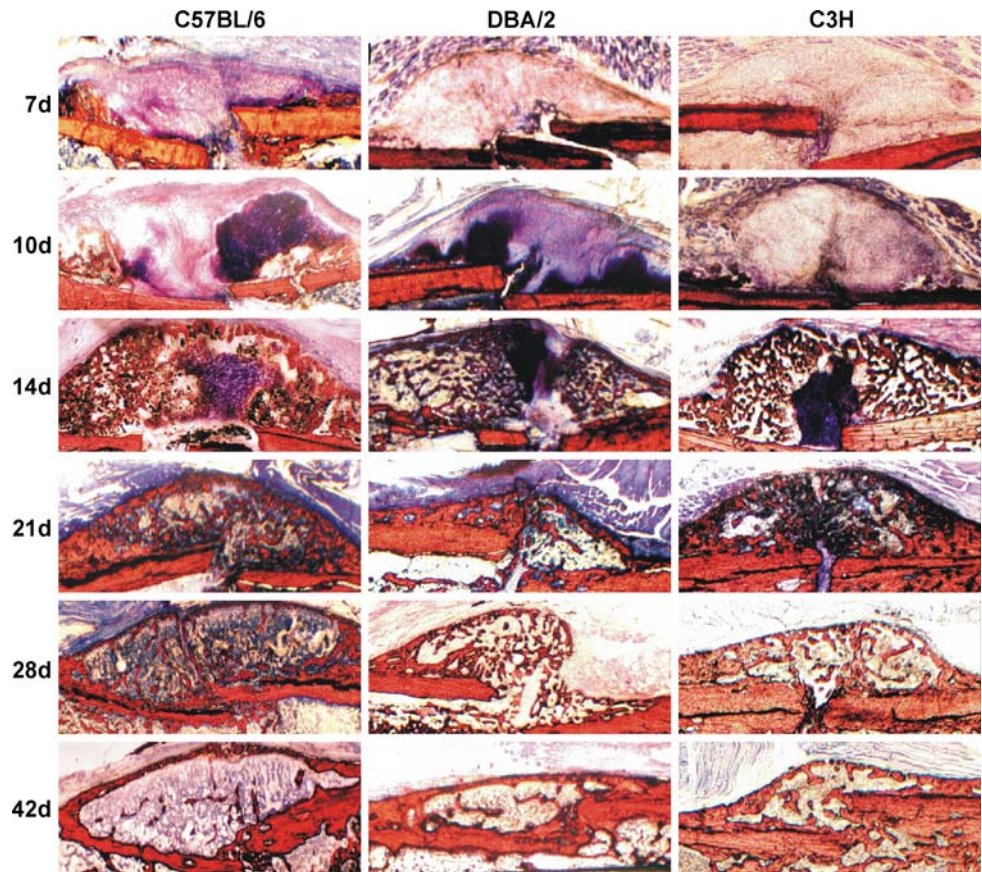

mineralized tissue (Fig. 3). Callus area peaked for all strains by 14 days after fracture and then slowly declined, consistent with fracture bridging between 2 and 3 weeks postfracture and callus remodeling (Fig. 3A). However, callus area in C57BL/6 mice was significantly greater than in either the DBA/2 or C3H strain at all time points except 7 days after fracture ($P \leq 0.007$ vs. DBA/2 and $P \leq 0.019$ vs. C3H for all time points). Callus area for C3H mice was significantly larger than for DBA/2 mice only at 10 and 42 days after fracture ($P < 0.001$ and $P = 0.018$, respectively). The amount of cartilage in the fracture callus appeared to peak at 10 days after fracture in all the strains and then to decline, with no or very little cartilage evident 4 weeks after fracture (Fig. 3B). However, cartilage persisted in the DBA/2 fracture callus longer than in the C57BL/6 or C3H calluses since there was significantly more cartilage in the calluses of the DBA/2 strain at 14 and 21 days after fracture ($P \leq 0.003$ vs. C57BL/6 or C3H at 14 days, $P = 0.005$ vs. C57BL/6 at 21 days, and $P = 0.047$ vs. C3H at 21 days). More new bone (percent mineralized tissue) was observed in the C57BL/6 calluses at 7 and 10 days after fracture than in the DBA/2 or C3H strains ($P < 0.001$ vs. either strain at both time points), consistent with the histological observations (Fig. 3C). The percent mineralized callus area peaked by 4 weeks after fracture in all strains examined.

To assess the rate at which endochondral ossification was proceeding in each strain, the percent cartilage area was multiplied by the percent mineralized tissue area to create an endochondral ossification index (Fig. 3D). Using this measure, the endochondral ossification index was higher during fracture repair in the C57BL/6 mice at 7 and 10 days after fracture compared to the DBA/2 or C3H mice ($P < 0.001$ vs. either strain at both time points). At 14 days after fracture, the endochondral ossification index was still higher in C57BL/6 calluses compared to C3H mice ($P = 0.012$). Consistent with the persistence of cartilage in the DBA/2 fracture callus, the endochondral ossification index was significantly higher in the DBA/2 fracture callus at 21 days postfracture compared to either the C57BL/6 or C3H mice ($P = 0.008$ vs. C57BL/6 and $P = 0.026$ vs. C3H).

Comparison of Fractured Femur Torsional Mechanical Strength Between Inbred Mouse Strains

Fracture repair was compared quantitatively between the inbred strains by biomechanical testing of the healing femurs. Torsional mechanical testing was performed on the right fractured femur and the left intact femur 4 weeks after fracture. This time point was chosen as it represents an early point after fracture bridging since it was anticipated
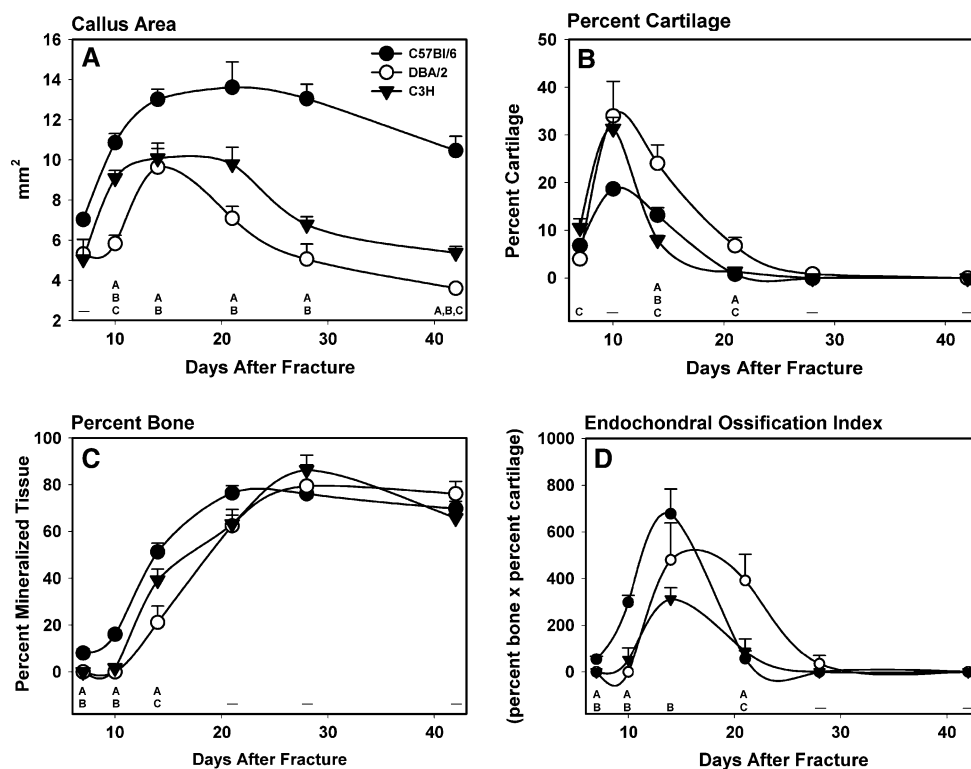
Fig. 3 Histomorphometric comparison of fracture healing between inbred mouse strains. Area measurements were made using ImagePro software from digital images captured for each fracture specimen. Fracture callus specimens were collected at 7, 10, 14, 21, 28, and 42 days after fracture. Callus area (**A**), percent cartilage area (**B**), percent mineralized tissue area (**C**), and endochondral ossification index (**D**) were measured or calculated. Shown are mean values for specimens from C57BL/6 (*filled circles*), DBA/2 (*open circles*), and

C3H (*inverted filled triangles*) mice. Error bars represent the standard error. Statistical comparisons were made within each time point, and significant differences ($P < 0.05$) are noted in each panel as (**A**) C57BL/6 vs. DBA/2, (**B**) C57BL/6 vs. C3H, and (**C**) DBA/2 vs. C3H for each time point. The numbers of specimens analyzed were 3, 4, 5, 5, 7, and 9 for C57BL/6; 3, 4, 3, 5, 4, and 8 for DBA/2; and 4, 4, 6, 4, 8, and 9 for C3H at each time point, respectively

that at later time points fracture healing would reach equivalence between all strains. To account for differences in animal weight, femur dimensions, and bone mineral density between the inbred strains, the mechanical testing data for each fractured right femur were normalized as the percentage value for its contralateral, intact left femur. For all structural and material parameters, the normalized values from C57BL/6 mice were significantly higher than those from DBA/2 or C3H mice (Fig. 4). While the normalized values obtained from DBA/2 mice were consistently higher than those from C3H mice, only maximum shear stress was significantly higher for DBA/2 mice compared to C3H mice.

In contrast to the normalized mechanical testing values for the fractured femurs, the intact femurs from C3H mice had the highest peak torque ($P < 0.001$), maximum rigidity ($P \leq 0.03$), maximum shear stress ($P < 0.001$), and shear modulus ($P < 0.005$, see Table 3). Despite the smaller dimensions of the DBA/2 femurs (Table 2), the structural properties of the DBA/2 femurs were similar to the larger-diameter C57BL/6 femurs. This appears to be due to the

increased material properties in DBA/2 mice since the maximum shear stress for C57BL/6 mice was significantly less than that for DBA/2 mice ($P < 0.001$) and the difference in shear modulus between these two strains approached statistical significance ($P = 0.081$).

Discussion

To the best of our knowledge, this is the first report comparing strain-dependent differences in fracture healing for any animal model. Other studies have compared ear punch wound-healing rates or drill-hole defects in tail vertebrae of mice [15, 16]. Unlike bone fractures, bone drill-hole defects heal by direct bone formation and not through an endochondral ossification pathway as fractures do [17, 18]. Healing of ear punch wounds involves formation of a blastema, in which chondrogenesis occurs as well as angiogenesis and epithelial proliferation [19]. While it is likely that certain regulatory genes controlling fracture healing, bone defect healing, and wound healing will be

Fig. 4 Comparison of torsional mechanical properties of healing femurs from different inbred mouse strains. Femurs were collected from mice 28 days after fracture and subjected to destructive torsional mechanical testing. To normalize for differences in bone morphology between strains, values are expressed as the percent ratio to the contralateral intact femur. Graphs show mean values for peak torque (**A**), maximum rigidity (**B**), maximum shear stress (**C**), and shear modulus (**D**) for C57BL/6, DBA/2, and C3H mice. Error bars show the standard error. Eleven pairs of femurs were tested for each strain. *P* values are shown in each graph and indicate significant differences compared to the C57BL/6 values except as noted in **C**
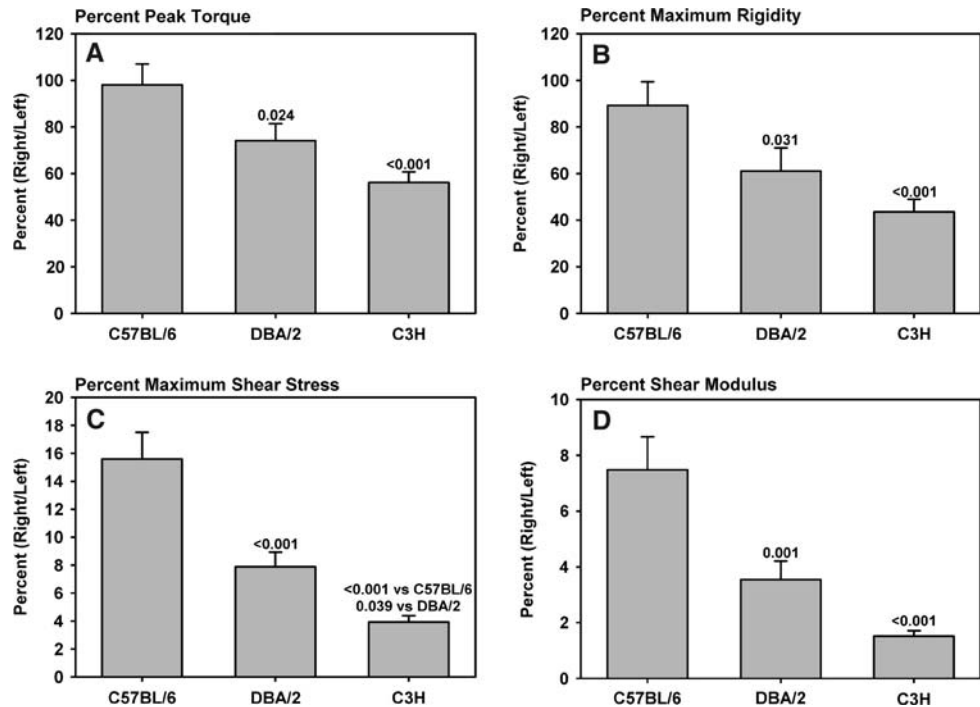
Table 3 Summary of mechanical testing results (mean ± SD)

	C57BL/6 ($n = 11$)	DBA/2 ($n = 11$)	C3H ($n = 11$)	All ($n = 33$)
Right fractured femurs				
Peak torque (N.mm)	31.8 ± 9.1	19.8 ± 6.3	21.5 ± 3.7	26.7 ± 8.5
Maximum rigidity (N.mm^2/rad)	835 ± 345	486 ± 187	543 ± 139	621 ± 280
Maximum shear stress (MPa)	15.2 ± 6.2	12.7 ± 6.6	9.6 ± 2.8	12.5 ± 5.8
Shear modulus (GPa)	0.22 ± 0.11	0.20 ± 0.12	0.15 ± 0.07	0.19 ± 0.11
Left intact femurs				
Peak torque (N.mm)	32.7 ± 3.8	27.3 ± 5.4	39.6 ± 6.7	35.9 ± 10.5
Maximum rigidity (N.mm^2/rad)	980 ± 401	906 ± 311	1,354 ± 434	1,081 ± 423
Maximum shear stress (MPa)	99.0 ± 20.9	158.3 ± 29.7	252.7 ± 48.8	170 ± 73
Shear modulus (GPa)	3.36 ± 1.88	6.08 ± 2.05	10.63 ± 5.46	6.69 ± 4.59

shared among these processes, many will not. Indeed, no correlation was found between the ability to heal an ear punch wound and a vertebral drill-hole defect among 10 different inbred mouse strains [16].

Fracture healing appears to proceed significantly faster in C57BL/6 mice compared to DBA/2 and C3H mice. This conclusion is based upon the presence of more mineralized tissue in the C57BL/6 callus sooner than the other strains (Figs. 2 and 3), a higher endochondral ossification index (Fig. 3D), and higher normalized biomechanical strength of the healing C57BL/6 femurs (Fig. 4). Speed of fracture healing appears to be inversely related to bone mineral density and the biomechanical properties of intact femurs from these mouse strains (Table 3) [8]. That fracture healing proceeds faster in C57BL/6 than in DBA/2 or C3H mice is surprising since previous studies have shown that osteoblasts from C3H mice are more active and have a

lower apoptosis rate than osteoblasts from C57BL/6 mice [20]. In addition, healing of drill-hole bone defects or ear punch wounds has been reported to be severely diminished in C57BL/6 mice [15, 16, 19]. This underscores the likelihood that different genetic regulatory pathways govern distinct tissue regenerative processes.

The fracture pattern shown in Fig. 1 for the C57BL/6 mouse was typical. Often, radiographs made immediately after fracture showed a diaphyseal, noncomminuted fracture. With time, however, comminutions developed or became evident in most C57BL/6 fractures. Bone quality is poor in C57BL/6 mice, and the development of comminutions likely reflects bone properties and not the fracture method. In support of this assertion, another study examining healing of vertebrae with drill-hole defects in C57BL/6 mice showed dramatic deformation of the vertebrae over a 30–day healing period [16].

Histological evidence indicated that new bone formed at the callus periphery of C57BL/6 mice sooner than for DBA/2 or C3H mice (Fig. 2). This suggests that bone formation initiates earlier in C57BL/6 mice. This was confirmed as increased new bone in the 7- and 10-day C57BL/6 fracture calluses (Fig. 3). However, this bone was not evident in the 7- and 10-day postfracture radiographs, suggesting that the new bone is poorly mineralized (Fig. 1). The C57BL/6 genotype may promote faster osteoid formation to bridge the fracture, with subsequent mineralization to consolidate healing. It also should be noted that the persistent increase in callus size of C57BL/6 mice may in part reflect the development of comminuted fractures. Thus, early histomorphometric measures may provide a more accurate assessment of healing in C57BL/6 mice.

A goal of this experiment was to identify a quantifiable trait that could be used to measure fracture healing between strains and potentially use this quantitative trait to identify genes that regulate bone regeneration. This required identifying inbred strains of mice that had sufficiently large differences in fracture healing capacity that the difference could be easily and reliably measured and identifying the most appropriate outcome measure. Radiographs are commonly used to assess fracture healing (Fig. 1). However, interpretation of radiographs has a very large subjective component and is unlikely to be a suitable quantitative measure [21, 22]. Torsional mechanical testing provided good quantitative outcome measures of fracture healing success (Fig. 4, Table 3). However, the variability inherent in this assay method required use of large sample sizes and, since it is a destructive test, the mice need to be killed prior to analysis. Thus, use of torsional mechanical testing would make any genetic approach to identifying genes involved in bone regeneration more difficult. Histomorphometric measures are labor-intensive and require killing the mice prior to analysis. However, the largest differences between strains were found using histomorphometric measures (Figs. 2 and 3); in particular, the endochondral ossification index would appear to be a particular relevant measure. Table 4 summarizes the magnitude of the differences between strains for the endochondral ossification index and torsional mechanical testing analysis. Table 4 also indicates the number of animals required to distinguish the parental phenotype using a t-test at each time point for the endochondral ossification index or for each mechanical parameter. Based upon this analysis, the endochondral ossification index could be used as a quantitative trait to identify genes that regulate fracture healing between C57BL/6 and DBA/2 or C3H mice during the early stages of healing since so few animals would be necessary to distinguish the parental phenotype. Further, the largest

Table 4 Summary of fracture healing endochondral ossification index and mechanical parameter differences between strains

Outcome measure	Percent difference[a]			Effect size[b]			Number of animals required to distinguish parental phenotype[c]		
	C57BL/6 vs. DBA/2	C57BL/6 vs. C3H	DBA/2 vs. C3H	C57BL/6 vs. DBA/2	C57BL/6 vs. C3H	DBA/2 vs. C3H	C57BL/6 vs. DBA/2	C57BL/6 vs. C3H	DBA/2 vs. C3H
EOI[d]: day 7	>5,000%	>5,000%	–	3.47 (0.94–6.00)	3.47 (1.11–5.82)	–	2	3	–
EOI: day 10	>25,000%	477%	–100%	7.07 (3.34–10.80)	2.92 (0.93–4.91)	–0.71 (–2.14 to 0.72)	1	4	60
EOI: day 14	41%	117%	54%	0.78 (–0.71 to 2.26)	1.96 (0.52–3.40)	0.79 (–0.64 to 2.22)	50	8	48
EOI: day 21	–86%	–36%	346%	–1.80 (–3.27 to –0.33)	–0.33 (–1.65 to 0.99)	1.57 (0.07–3.07)	10	274	13
Peak torque	32%	75%	32%	0.89 (0.01–1.77)	1.80 (0.81–2.79)	0.89 (0.01–1.76)	38	10	38
Max. rigidity	46%	105%	40%	0.84 (–0.03 to 1.72)	1.69 (0.72–2.67)	0.65 (–0.20 to 1.51)	42	11	70
Max. shear stress	97%	300%	103%	1.49 (0.55–2.44)	2.52 (1.40–3.64)	1.49 (0.54–2.43)	14	5	14
Shear modulus	114%	400%	133%	1.26 (0.35–2.18)	2.15 (1.10–3.20)	1.24 (0.33–2.15)	19	7	20

[a] [(mean$_a$ – mean$_b$)/mean$_b$] × 100%

[b] Effect size (Cohen's d) = (mean$_a$ – mean$_b$)/$\sqrt{[(\sigma_a^2 + \sigma_b^2)/2]}$, where σ is the SD, with 95% confidence intervals in parentheses

[c] Required group size estimated using power of 0.9, 99% confidence, and the pooled variation for that assay or time point

[d] Endochondral ossification index

effect size was found when comparing the endochondral ossification index between C57BL/6 and DBA/2 mice at 10 days after fracture. If the difference in fracture healing capacity between the C57BL/6 and DBA/2 strains is regulated by more than one genetic locus, then choosing that outcome measure that provides the largest effect size would be optimal for any future quantitative trait locus mapping strategy. In contrast, analysis of the mechanical testing data found smaller effect sizes between strains, with concomitantly larger group sizes necessary to distinguish parental phenotypes.

Histomorphometric methods as described here could be used to measure the endochondral ossification index for a quantitative trait locus analysis. However, new methods that rapidly quantify callus cartilage and new bone area in living animals also would enable use of the endochondral ossification index to identify quantitative trait loci that affect bone regeneration. Indeed, use of newer imaging methods to detect luciferase or fluorescent proteins in living mice may enable development of a successful genetic screen [23–26]. For instance, transgenes that direct expression of different luciferase enzymes (firefly vs. sea pansy) in newly formed bone and cartilage could be used to measure callus bone and cartilage in a living mouse, obtain the endochondral ossification index, and keep the animal alive for subsequent breeding. Similarly, newly formed bone could be labeled with a far-red fluorescent pamidronate and, in combination with chondrocyte-specific luciferase expression, used to determine the endochondral ossification index in living mice [27, 28].

One limitation of this study is the fracture model. Fractures were produced in all mice using the same materials and procedures. However, the diameter of the intramedullary canal varies significantly between C57BL/6, DBA/2, and C3H mice. Thus, the possible amount of movement across the fracture gap (intramedullary canal diameter less fixation pin diameter) would be different for each strain. This could alter the mechanical stress experienced by the cells at the fracture site and alter the healing response. Fixation pins of different diameters could be used to maintain a constant possible amount of movement across the fracture gap. However, the pins would need to be of different materials in order to keep the stiffness of the fixation pin constant. Another approach would be to use an internal or external plate attached proximal and distal to the fracture to stabilize the fracture site [29, 30]. In this case, movement across the fracture gap would be primarily a function of plate stiffness.

In summary, the data demonstrate that significant differences in fracture healing occur between three inbred strains of mice and support the hypothesis that specific genetic determinants regulate bone regeneration. There is sufficient difference in bone regeneration between inbred strains that a genetic approach to identify genes regulating bone regeneration is warranted.

References

1. Gerstenfeld LC, Cullinane DM, Barnes GL, Graves DT, Einhorn TA (2003) Fracture healing as a post-natal developmental process: molecular, spatial, and temporal aspects of its regulation. J Cell Biochem 88:873–884
2. Simon AM, Manigrasso MB, O'Connor JP (2002) Cyclo-oxygenase 2 function is essential for bone fracture healing. J Bone Miner Res 17:963–976
3. Simon AM, O'Connor JP (2007) Dose and time-dependent effects of cyclooxygenase-2 inhibition on fracture-healing. J Bone Joint Surg Am 89:500–511
4. Gerstenfeld LC, Cho TJ, Kon T, Aizawa T, Tsay A, Fitch J, Barnes GL, Graves DT, Einhorn TA (2003) Impaired fracture healing in the absence of TNF-alpha signaling: the role of TNF-alpha in endochondral cartilage resorption. J Bone Miner Res 18:1584–1592
5. Hausman MR, Schaffler MB, Majeska RJ (2001) Prevention of fracture healing in rats by an inhibitor of angiogenesis. Bone 29:560–564
6. Maes C, Carmeliet P, Moermans K, Stockmans I, Smets N, Collen D, Bouillon R, Carmeliet G (2002) Impaired angiogenesis and endochondral bone formation in mice lacking the vascular endothelial growth factor isoforms VEGF$_{164}$ and VEGF$_{188}$. Mech Dev 111:61–73
7. Lander ES, Botstein D (1989) Mapping mendelian factors underlying quantitative traits using RFLP linkage maps. Genetics 121:185–199
8. Beamer WG, Donahue LR, Rosen CJ, Baylink DJ (1996) Genetic variability in adult bone density among inbred strains of mice. Bone 18:397–403
9. Bak B, Andreassen TT (1989) The effect of aging on fracture healing in the rat. Calcif Tissue Int 45:292–297
10. Meyer RA Jr, Tsahakis PJ, Martin DF, Banks DM, Harrow ME, Kiebzak GM (2001) Age and ovariectomy impair both the normalization of mechanical properties and the accretion of mineral by the fracture callus in rats. J Orthop Res 19:428–435
11. Lu C, Miclau T, Hu D, Hansen E, Tsui K, Puttlitz C, Marcucio RS (2005) Cellular basis for age-related changes in fracture repair. J Orthop Res 23:1300–1307
12. Manigrasso MB, O'Connor JP (2004) Characterization of a closed femur fracture model in mice. J Orthop Trauma 18:687–695
13. Baron R, Vigney A, Neff L, Silvergate A, Santa Maria A (1983) Processing of undecalcified bone specimens for bone histomorphometry. In: Recker RR (ed) Bone histomorphometry: techniques and interpretation. CRC Press, Boca Raton, FL, pp 13–35
14. Maniatopoulos C, Rodriguez A, Deporter DA, Melcher AH (1986) An improved method for preparing histological sections of metallic implants. Int J Oral Maxillofac Implants 1:31–37
15. Li X, Gu W, Masinde G, Hamilton-Ulland M, Xu S, Mohan S, Baylink DJ (2001) Genetic control of the rate of wound healing in mice. Heredity 86:668–674
16. Li X, Gu W, Masinde G, Hamilton-Ulland M, Rundle CH, Mohan S, Baylink DJ (2001) Genetic variation in bone-regenerative capacity among inbred strains of mice. Bone 29:134–140
17. Nagashima M, Sakai A, Uchida S, Tanaka S, Tanaka M, Nakamura T (2005) Bisphosphonate (YM529) delays the repair of cortical bone defect after drill-hole injury by reducing terminal differentiation of osteoblasts in the mouse femur. Bone 36:502–511
18. Chiba S, Okada K, Lee K, Segre GV, Neer RM (2001) Molecular analysis of defect healing in rat diaphyseal bone. J Vet Med Sci 63:603–608

19. Rajnoch C, Ferguson S, Metcalfe AD, Herrick SE, Willis HS, Ferguson MW (2003) Regeneration of the ear after wounding in different mouse strains is dependent on the severity of wound trauma. Dev Dyn 226:388–397

20. Sheng MH, Lau KH, Mohan S, Baylink DJ, Wergedal JE (2006) High osteoblastic activity in C3H/HeJ mice compared to C57BL/6J mice is associated with low apoptosis in C3H/HeJ osteoblasts. Calcif Tissue Int 78:293–301

21. Panjabi MM, Lindsey RW, Walter SD, White AA III (1989) The clinician's ability to evaluate the strength of healing fractures from plain radiographs. J Orthop Trauma 3:29–32

22. Blokhuis TJ, de Bruine JH, Bramer JA, den Boer FC, Bakker FC, Patka P, Haarman HJ, Manoliu RA (2001) The reliability of plain radiography in experimental fracture healing. Skeletal Radiol 30:151–156

23. de Boer J, van Blitterswijk C, Lowik C (2006) Bioluminescent imaging: emerging technology for non-invasive imaging of bone tissue engineering. Biomaterials 27:1851–1858

24. Iris B, Zilberman Y, Zeira E, Galun E, Honigman A, Turgeman G, Clemens T, Gazit Z, Gazit D (2003) Molecular imaging of the skeleton: quantitative real-time bioluminescence monitoring gene expression in bone repair and development. J Bone Miner Res 18:570–578

25. Yang M, Baranov E, Jiang P, Sun FX, Li XM, Li L, Hasegawa S, Bouvet M, Al-Tuwaijri M, Chishima T, Shimada H, Moossa AR, Penman S, Hoffman RM (2000) Whole-body optical imaging of green fluorescent protein-expressing tumors and metastases. Proc Natl Acad Sci USA 97:1206–1211

26. Yang M, Li L, Jiang P, Moossa AR, Penman S, Hoffman RM (2003) Dual-color fluorescence imaging distinguishes tumor cells from induced host angiogenic vessels and stromal cells. Proc Natl Acad Sci USA 100:14259–14262

27. Zaheer A, Lenkinski RE, Mahmood A, Jones AG, Cantley LC, Frangioni JV (2001) In vivo near-infrared fluorescence imaging of osteoblastic activity. Nat Biotechnol 19:1148–1154

28. Kozloff KM, Weissleder R, Mahmood U (2007) Noninvasive optical detection of bone mineral. J Bone Miner Res 22:1208–1216

29. Cheung KM, Kaluarachi K, Andrew G, Lu W, Chan D, Cheah KS (2003) An externally fixed femoral fracture model for mice. J Orthop Res 21:685–690

30. Connolly CK, Li G, Bunn JR, Mushipe M, Dickson GR, Marsh DR (2003) A reliable externally fixated murine femoral fracture model that accounts for variation in movement between animals. J Orthop Res 21:843–849